Applied Physics Letters

High sensitivity hexagonal boron nitride lateral neutron detectors

Cite as: Appl. Phys. Lett. **114**, 222102 (2019); https://doi.org/10.1063/1.5098331
Submitted: 01 April 2019 . Accepted: 12 May 2019 . Published Online: 04 June 2019

A. Maity, S. J. Grenadier, J. Li, J. Y. Lin, and H. X. Jiang

AIP Publishing

Applied Physics Letters ARTICLE scitation.org/journal/apl

High sensitivity hexagonal boron nitride lateral neutron detectors

Cite as: Appl. Phys. Lett. **114**, 222102 (2019); doi: 10.1063/1.5098331
Submitted: 1 April 2019 · Accepted: 12 May 2019 ·
Published Online: 4 June 2019

A. Maity, S. J. Grenadier, J. Li, J. Y. Lin, and H. X. Jiang[a]

AFFILIATIONS

Department of Electrical and Computer Engineering, Texas Tech University, Lubbock, Texas 79409, USA

[a]Email: hx.jiang@ttu.edu

ABSTRACT

Hexagonal boron nitride (h-BN) thermal neutron detectors have demonstrated the highest detection efficiency among all solid-state detectors (at 58% for a detection area of 1 mm^2 and 53% for a detection area of 9 mm^2). However, scaling up the detector size of vertical h-BN detectors is challenging due to increased dark current, capacitance, and surface recombination with the increasing detection area. Here, we report the demonstration of a 29 mm^2 thermal neutron detector fabricated from a freestanding ^{10}B enriched h-BN epilayer of 90 μm in thickness with a detection efficiency of 50% by employing a lateral device geometry. The lateral detector geometry takes advantage of the unique layered structure of h-BN which naturally provides higher in-plane carrier mobilities than those in the vertical direction. Moreover, due to the reduced area of metals in contact with the h-BN material, the detrimental effects associated with the surface recombination at the metal contacts and device capacitance were reduced, which resulted in improved charge collection efficiency and signal to noise ratios. This work laid the ground work for scaling up to large size neutron detectors based on h-BN.

Neutron radiation is a signature of the presence of special nuclear materials like plutonium-239 (^{239}Pu). Hence, detectors for sensing neutron radiation are an indispensable tool for detecting any illicit movement of fissile materials at the ports of entry.[1] Neutron detectors are also essential for geothermal and well-logging applications in determining the formation properties of rocks like the water content and porosity.[2] The most technologically mature and widely deployed neutron detectors are pressurized gas detectors filled with helium-3 (^3He) which has a high thermal neutron capture cross-section of ~5330 b.[3] However, these detectors are inherently bulky due to long absorption lengths for thermal neutrons in a low atomic density gas filled neutron absorption medium. Other disadvantages of ^3He detectors include high biasing voltage (>1000 V), low Q value (~0.764 MeV), high ionization energy of the gas, slow response speed (~ms), high pressurization, and high cost. Therefore, solid-state neutron detectors with high efficiencies and sensitivities with the potential to replace helium-3 gas-filled neutron detectors are an important emerging technology.

Hexagonal boron nitride (h-BN), a wide bandgap ($E_g > 6.0$ eV) semiconductor, well known for its deep UV applications, has emerged as a highly efficient material for the fabrication of solid-state neutron detectors.[4–10] The boron-10 (^{10}B) isotope having a large thermal neutron capture cross-section ($\sigma \sim 3840$ b $= 3.84 \times 10^{-21}$ cm^2) along with a high atomic density (N) in 100% ^{10}B-enriched h-BN (h-^{10}BN) of ~$5.5 \times 10^{22}/cm^3$ provides a large thermal neutron absorption cross section (α) and hence a short thermal neutron absorption length (λ) in h-^{10}BN of ~47.3 μm [$\lambda = \alpha^{-1} = (N\sigma)^{-1} = (5.5 \times 10^{22} \times 3.84 \times 10^{-21})^{-1}$ cm].[7] Other advantages of h-^{10}BN include higher temperature handling capability, reduced size and weight, no pressurization, and lower operating voltage over those of ^3He gas detectors. Furthermore, due to the low atomic numbers of boron and nitrogen atoms, h-^{10}BN has a low sensitivity to gamma radiation.[7]

Vertical h-^{10}BN photoconductive-type thermal neutron detectors consisting of a pair of planar metal contacts deposited on the top and bottom surfaces have demonstrated the highest detection efficiency among all solid-state detectors (at 58% for a detection area of 1 mm^2 and 53% for a detection area of 9 mm^2) and a gamma rejection ratio of better than 10^{-6}, attributed primarily to the ability for producing thick (~50 μm) films by metal organic chemical vapor deposition (MOCVD).[8,9] However, neutron flux from a primitive nuclear device is usually low (~3×10^5 neutrons/s), and therefore, large size neutron detectors are desired for practical applications along with high efficiency. There are several technical challenges to scale up the device size while maintaining a high detection efficiency. Increasing the detector size of vertical detectors tends to excessively increase the (a) dark current, (b) capacitance, and (c) surface recombination. Associated with high dark current and capacitance is a decrease in the signal to noise ratio, resulting in low detection efficiency.[8,11] Surface recombination is another key limiting factor for attaining high charge

collection efficiency in vertical detectors due to the presence of charge traps located at the metal-BN interface. Previous studies have shown that the surface recombination field increases with the increasing detector size.[12,13] As a result of these effects combined, the overall detection efficiency in vertical photoconductive-type detectors decreases dramatically with the increasing device size. In this work, we report an alternative approach for fabricating h-^{10}BN detectors in a lateral geometry with the aim of overcoming the challenges involved in the vertical detectors and realization of a 29 mm^2 detector with a thermal neutron detection efficiency of about 50%.

Epilayers of h-^{10}BN of 90 μm in thickness were grown using MOCVD on 4 in. c-plane sapphire substrates. The detailed growth conditions were discussed previously.[7–9,13,15] The unique layered structure of h-BN coupled with different thermal expansion coefficients between h-BN and the sapphire substrate enables a natural separation of thick h-BN layers from sapphire substrates after growth during cooling down as schematically illustrated in Fig. 1(a). An optical image of a 90 μm thick freestanding h-^{10}BN wafer of 4 in. in diameter is shown in Fig. 1(b). The wafer was then diced for detector fabrication. In this study, we combined two strips with dimensions of 1.2 mm in width and 14 and 10 mm in length to form a photoconductive-type lateral detector with a total device area of 28.8 mm^2. The strips were mounted on a host sapphire using a highly resistive adhesive material so that the bottom surface of h-^{10}BN faces radiation. A mask of 1 mm in width was used to deposit ohmic contacts consisting of a bilayer of Ni (100 nm)/Au (40 nm) on the clipped edges of the h-^{10}BN strips using e-beam evaporation, leaving around ~100 μm of metal covering on the edges, as schematically depicted in Fig. 1(c). Optical image of a fabricated h-^{10}BN lateral detector is shown in Fig. 1(d). Photocurrent-voltage characteristics under UV excitation were characterized to obtain the mobility-lifetime products ($\mu\tau$) and surface recombination field E_S (=s/μ), defined as the ratio of the surface recombination velocity (s) to the carrier mobility (μ).[12,13] The neutron detection efficiency was determined by comparing the neutron counts obtained from the h-^{10}BN detector with a commercially purchased ^{6}LiF filled microstructured semiconductor neutron detector (MSND Domino™ V4) under thermal neutron irradiation from a depleted ^{252}Cf (Claifonium-252) source, as previously described.[7–9]

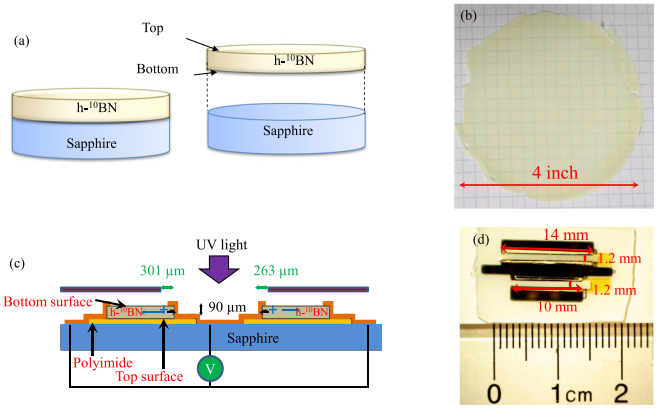

FIG. 1. (a) Schematic diagram of the separation process for obtaining freestanding h-^{10}BN epilayers. (b) Optical image of a freestanding h-^{10}BN wafer of 4 in. in diameter. (c) Schematic diagram of a lateral detector mounted on an insulating mount (sapphire) with a small area near one of its metal contacts illuminated with UV radiation allowing the probing of transport properties for electrons and holes separately. (d) Optical image of a 28.8 mm^2 neutron detector fabricated from a freestanding h-^{10}BN of 90 μm in thickness.

As the charge carrier mobility-lifetime product ($\mu\tau$) and surface recombination field E_S (=s/μ) are two of the most important parameters for determining the charge collection efficiency of h-BN detectors,[12,13] the photocurrent-voltage characteristics under UV excitation were measured to extract these parameters using Many's equation[12]

$$I_i(V) = I_{0,i}\eta_{c,i} = I_{0,i}\left[\frac{V_b\mu_i\tau_i\left(1-e^{-\frac{W^2}{V_b\mu_i\tau_i}}\right)}{W^2\left(1+\frac{s_iW}{\mu_iV_b}\right)}\right] \quad (i=e,\,h). \qquad (1)$$

Here, η_c defines the charge collection efficiency, I_0 is the saturation current, $\mu_h\tau_h$ ($\mu_e\tau_e$) and s_h (s_e) denote the mobility-lifetime product and surface recombination velocity for holes (electrons), respectively, and V_b is the bias voltage applied to the two metal contacts giving an applied electric field of $E_a = V_b/W$, with W being the distance between two electrodes. Equation (1) implies that in order to achieve a high charge collection efficiency, the following two conditions must be satisfied: (a) $\frac{W^2}{\mu\tau V_b} = \frac{W}{\mu\tau E_a} \ll 1$, which simply states that the charge carrier drift length (=$\mu\tau E_a$) needs to be much larger than the carrier transit distance, W, and (b) $\frac{s/\mu}{V_b/W} = \frac{Es}{E_a} \ll 1$, which means that the external applied electric field must be greater than the surface recombination field, $E_a \gg E_s$, in order to effectively sweep out charge carriers.[12,13]

Figures 2(a) and 2(b) show the photocurrent vs V_b under UV radiation for both hole and electron transport. A deuterium UV lamp (DS421, Acton Research Corporation) was used as the light source

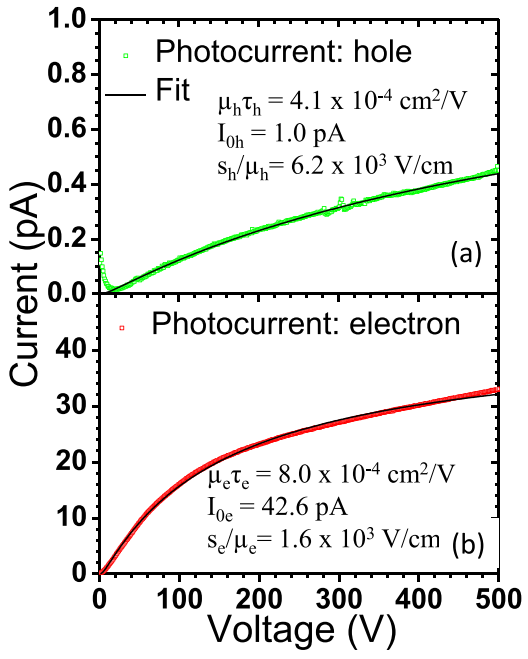

FIG. 2. Photocurrent-voltage characteristics of a lateral h-^{10}BN detector under UV excitation for (a) hole and (b) electron transport.

covering a spectral range of 190–350 nm. A metal slit was used to selectively illuminate near only one metal contact, as illustrated in Fig. 1(c). If the electrode near the illuminated area is positively (negatively) biased, holes (electrons) travel a much longer distance compared to electrons (holes) before being collected at the electrodes. This scheme enables us to measure the photocurrent for holes or electrons separately, as shown in Figs. 2(a) and 2(b). By fitting the photocurrent-voltage characteristics with Eq. (1), values of $\mu\tau$ and s/μ were extracted to be $\mu_h\tau_h = 4.1 \times 10^{-4}$ cm^2/V, $\mu_e\tau_e = 8.0 \times 10^{-4}$ cm^2/V, $s_h/\mu_h = 6.2 \times 10^3$ V/cm, and $s_e/\mu_e = 1.6 \times 10^3$ V/cm. The results imply that our lateral h-^{10}BN detector has a value of $\frac{W^2}{\mu\tau V_b} = \frac{W}{\mu\tau E_a} \leq 0.06$ at a bias voltage of $V_b = 550$ V for both electron and hole transports, well satisfying the condition for a high charge collection efficiency. The measured values for $\frac{s_h/\mu_h}{V_b/W} = \frac{E_s^h}{E_a} \approx 1.35$ and $\frac{s_e/\mu_e}{V_b/W} = \frac{E_s^e}{E_a} \approx 0.35$ at a bias voltage of 550 V, which are short from the ideal conditions for a high charge collection efficiency. These values together provide a total charge collection efficiency for electrons (holes) of 72.9%, (41.2%) at a bias voltage of 550 V. In comparison, vertical detectors of a similar size exhibit a typical charge collection efficiency below 30% under the same electric field. Nevertheless, the results clearly show that it is the surface recombination which limits the charge collection efficiency in lateral h-^{10}BN detectors.

Pulse height spectra of the lateral h-^{10}BN detector were measured at different bias voltages (V_b) under thermal neutron radiation from a ^{252}Cf source with a radioactivity of 0.50 mCi ($\sim 2.14 \times 10^6$ n/s) moderated by a high-density polyethylene (HDPE) block of 2.5 cm in thickness.[6–9] Pulse height spectra were first recorded for 15 min in the absence of any source where the highest channel of this dark spectrum recorded for each V_b acted as a low-level discriminator (LLD). Then, the detector was exposed to thermal neutrons at 60 cm away from the HDPE moderated ^{252}Cf source under the same V_b for 15 min to obtain the pulse height spectra, as shown in Fig. 3. The total number of neutron counts was obtained by integrating the pulse height spectrum beyond the LLD. By comparing the counts from a ^{6}LiF filled microstructured semiconductor neutron detector (MSND Domino V4) with a thermal neutron detection efficiency of 30 (±1)% and a device area of 4 cm^2, the detection efficiency (η) of our h-^{10}BN lateral detector was determined to be 49.5 (±2.2)% at a bias voltage of 550 V. In terms of the detection sensitivity, $C_R \propto \eta A$, this lateral detector outperforms the previous state-of-the-art 9 mm^2 vertical detectors by a factor of about 3 [=(50% × 29 mm^2)/(53% × 9 mm^2)].[8]

Neutrons are not only incident randomly on the c-plane in-between two electrodes of the h-^{10}BN detector, but they are also absorbed randomly deeper inside the detector due to a longer absorption length of $\lambda \sim 47.3$ μm for thermal neutrons than for the above bandgap photons of ~13 nm in h-^{10}BN. Moreover, in contrast to photocurrent, neutrons are detected one at a time. Therefore, the charge collection efficiency (η_c) under neutron excitation may not be identical to those measured under UV photon excitation. Figure 4 plots η_c vs V_b for the lateral h-^{10}BN detector under thermal neutron irradiation, where η_c accounts for the discrepancy between the measured thermal neutron detection efficiency (η) and the theoretical detection efficiency, $p(t) = 1 - e^{\frac{-t}{\lambda}} = 85\%$ for a detector with a thickness of $t = 90$ μm, and can be calculated from the ratio of η/p.[7] The results shown in Fig. 4 indicate that this device requires at least 100 V to have any sensitivity to neutrons. This could be due to a potential drop at the semiconductor-metal junction. Moreover, η_c starts to saturate at $V_b \sim 400$ V and approaches a value of 58.2 (±2.6)% at 550 V.

Although the charge collection efficiencies of h-^{10}BN lateral neutron detectors are still primarily limited by the surface effects, they are significantly improved over those in vertical detectors with the same detection area. However, compared to a vertical detector of the same detection area consisting of a pair of planar metal contacts deposited on the top and bottom surfaces,[7–9] lateral detectors possess several other advantageous features as presented in Table I. The lateral or in-plane mobility ($\mu_\perp$) of charge carriers is estimated to be ~100 times greater than that in the vertical direction, $\mu_{||}$.[14] High carrier mobility is

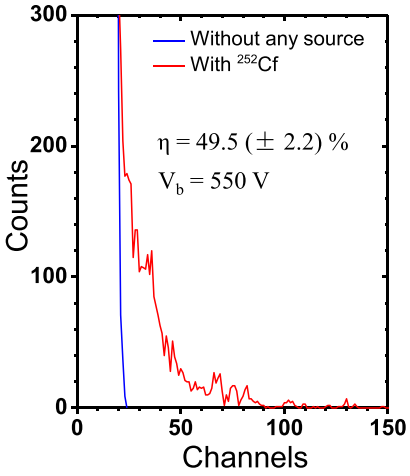

FIG. 3. Nuclear reaction pulse height spectrum of the 28.8 mm^2 lateral h-^{10}BN detector under thermal neutron radiation. The neutron response was measured by placing the detector 60 cm away from the ^{252}Cf source moderated by a 1 in. thick high-density polyethylene (HDPE) moderator for 15 min. To determine the "dark" counts or electronic noise level at this distance, another measurement was conducted for 15 min at the same bias voltage in the absence of any source (blue curve).

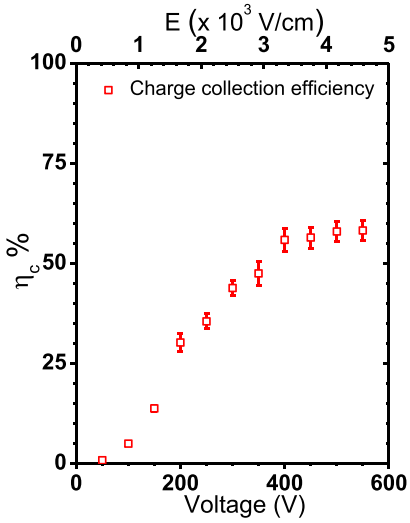

FIG. 4. Bias voltage dependence of the charge collection efficiency of a 28.8 mm^2 lateral h-^{10}BN detector under thermal neutron irradiation.

TABLE I. A qualitative comparison of important device parameters between vertical and lateral h-BN detectors.

Quantity	Vertical (|| to the c-axis)	Lateral ($\perp$ to c-axis)	Ratio of vertical to lateral (ratio || to $\perp$)
Assuming a detector width of W = 1.2 mm, a length of L = 14 mm, a thickness of t = 90 μm, $\varepsilon_{\|\|} = 5.06$, and $\varepsilon_{\perp} = 6.85$ (Ref. 16)			
Mobility	$\mu_{\|\|}$	$\mu_{\perp}$	$\mu_{\|\|}/\mu_{\perp} \sim 0.01$ (Ref. 14)
Resistivity ρ	$1/pe\mu_{\|\|}$	$1/pe\mu_{\perp}$	$\mu_{\perp}/\mu_{\|\|} \sim 100$
Resistance R	$\rho_{\|\|}$ (t/LW)	$\rho_{\perp}$ (W/Lt)	$(\mu_{\perp}/\mu_{\|\|})(t^2/W^2) \sim 0.6$
Capacitance C	$\varepsilon_{\|\|}$ (LW/t)	$\varepsilon_{\perp}$ (Lt/W)	$(\varepsilon_{\|\|}/\varepsilon_{\perp})(W^2/t^2) \sim 1.3 \times 10^2$
RC constant	$\rho_{\|\|}\,\varepsilon_{\|\|}$	$\varepsilon_{\perp}\rho_{\perp}$	$(\mu_{\perp}/\mu_{\|\|})(\varepsilon_{\|\|}/\varepsilon_{\perp}) \sim 0.8 \times 10^2$
Surface recombination	$\propto$ LW	$\propto$ Lt	$\sim$ W/t $\sim$ 13.3
Electric field E_a	V_b/t	V_b/W	W/t $\sim$ 13.3
Metal deposition	2 times	1 time	

expected to benefit the charge collection efficiency.[13] The resistivity of lateral devices is ~100 times lower than that of vertical devices. However, the separation distance between the electrodes is farther apart in the lateral detector (detector width, W) compared to that in the vertical detector (detector thickness, *t*), providing a larger resistance, R. Moreover, while the cross-section area for neutron radiation along the c-axis of h-^{10}BN is the same, the cross-section area for charge carrier collection (or the contact area) in a lateral detector shown schematically in Fig. 1(c) is significantly reduced, providing a reduced capacitance, *C*. This is the reason why the measured dark current (I_d) for the lateral detector investigated here was <0.1 pA at a bias voltage $V_b > 500$ V, which is considerably lower than that in the vertical h-BN detector of the same size, whereas the *C* and the *RC* time constant of the lateral detector are about two orders of magnitude smaller than those of the vertical detector. The reductions in I_d and *C* significantly improve the detection efficiency since the electronic noise (or LLD) decreases linearly with decreasing I_d and quadratically with decreasing *C*.[11] Also, the number of surface traps in a lateral detector is lower at the metal-BN interface due to the reduced area of metals in contact with h-^{10}BN. Hence, the surface effects are reduced, which in turn would enhance the charge collection efficiency in lateral detectors.[13] These combined advantages enabled us to increase the detector size while maintaining a high detection efficiency of 50% in lateral detectors. Furthermore, in terms of fabrication processes, lateral detectors require only one-time metal deposition compared to two times for vertical detectors, reducing the processing steps and thereby potentially increasing the device yield.

In summary, we have fabricated a lateral h-^{10}BN detector with a device size of 29 mm^2 with a detection efficiency of about 50%. Our work showed that it is easier to fabricate and scale up the size of detectors in a lateral geometry compared to vertical geometry. This is due to unique features of the layered structure of h-BN as well as decreased capacitance and surface recombination effects in lateral devices. However, improvements in metal contact fabrication and surface treatment processes are needed to minimize the surface effects. This work laid the foundation for the development of larger area h-^{10}BN detectors with high efficiency and sensitivity.

This research is supported by DOE ARPA-E (No. DE-AR0000964). The NNSA SSAA program (No. DE-NA0002927) supported the initial efforts of detector fabrication. Jiang and Lin are grateful to the AT&T Foundation for the support of Ed Whitacre and Linda Whitacre endowed chairs.

REFERENCES

[1]W. A. Noonan, Johns Hopkins APL Tech. Dig. **32**, 762 (2014).
[2]J. Neal, L. Boatner, Z. Bell, H. Akkurt, and M. McCarthy, "Evaluation of neutron and gamma detectors for high-temperature well-logging applications," in Future of Instrumentation International Workshop (FIIW) (2011), pp. 172–175.
[3]G. F. Knoll, *Radiation Detection and Measurement*, 4th ed. (John Wiley & Sons, 2010).
[4]J. Li, R. Dahal, S. Majety, J. Y. Lin, and H. X. Jiang, Nucl. Instrum. Methods Phys. Res., Sect. A **654**, 417 (2011).
[5]T. C. Doan, S. Majety, S. Grenadier, J. Li, J. Y. Lin, and H. X. Jiang, Nucl. Instrum. Methods Phys. Res., Sect. A **748**, 84 (2014); **783**, 121 (2015).
[6]T. C. Doan, J. Li, J. Y. Lin, and H. X. Jiang, AIP Adv. **6**, 075213 (2016).
[7]A. Maity, T. C. Doan, J. Li, J. Y. Lin, and H. X. Jiang, Appl. Phys. Lett. **109**, 072101 (2016).
[8]A. Maity, S. J. Grenadier, J. Li, J. Y. Lin, and H. X. Jiang, Appl. Phys. Lett. **111**, 033507 (2017).
[9]A. Maity, S. J. Grenadier, J. Li, J. Y. Lin, and H. X. Jiang, J. Appl. Phys. **123**, 044501 (2018).
[10]K. Ahmed, R. Dahal, A. Weltz, J. J. Q. Lu, Y. Danon, and I. B. Bhat, Appl. Phys. Lett. **110**, 023503 (2017).
[11]H. G. Spieler and E. E. Haller, IEEE Trans. Nucl. Sci. **32**, 419 (1985).
[12]A. Many, J. Phys. Chem. Solids **26**, 575 (1965).
[13]A. Maity, S. J. Grenadier, J. Li, J. Y. Lin, and H. X. Jiang, J. Appl. Phys. **125**, 104501 (2019).
[14]R. Dahal, K. Ahmed, J. W. Wu, A. Weltz, J. J.-Q. Lu, Y. Danon, and I. B. Bhat, Appl. Phys. Express **9**, 065801 (2016).
[15]S. J. Grenadier, A. Maity, J. Li, J. Y. Lin, and H. X. Jiang, Appl. Phys. Lett. **112**, 162103 (2018).
[16]R. Geick, C. H. Perry, and G. Rupprecht, Phys. Rev. **146**, 543 (1966).